Cement and Concrete Research 40 (2010) 1582–1589

Contents lists available at ScienceDirect

Cement and Concrete Research

journal homepage: http://ees.elsevier.com/CEMCON/default.asp

Dependency of C–S–H carbonation rate on CO_2 pressure to explain transition from accelerated tests to natural carbonation

N. Hyvert [a,b], A. Sellier [a,*], F. Duprat [a], P. Rougeau [b], P. Francisco [b]

[a] Université de Toulouse, UPS, INSA, LMDC (Laboratoire Matériaux et Durabilité des Constructions), 135, avenue de Rangueil, F-31 077 Toulouse CEDEX 04, France
[b] CERIB (Studies and Research Center for the Precast Industries), BP 30059, 28231 Epernon CEDEX, France

ARTICLE INFO

Article history:
Received 1 April 2009
Accepted 28 June 2010

Keywords:
Cement
Carbonation
CO_2 pressure
Characterization
Modeling

ABSTRACT

The use of normalized accelerated carbonation tests is currently limited to the classification of concretes in terms of carbonation resistance and the results are not easily transposable to forecasting concrete carbonation in natural conditions. Common models assume that the kinetics of the carbonation front ingress in concrete is a square root function of the CO_2 pressure but observations in the field generally invalidate this assumption. Based on an experimental program including carbonation tests at several CO_2 pressures, this paper shows that the amount of carbonated product depends largely on the CO_2 pressure. Several experimental analyses of carbonated concrete under different pressures are confronted, to finally propose a new analytical model able to predict carbonation ingress in natural conditions using the results of accelerated tests. The model takes both the cement chemical composition and its amount in concrete into account. The carbonation kinetics dependence on CO_2 pressure is considered through two underlying functions including, for the first, the dependence of the CSH carbonation rate on the pressure and, for the second, the effect of this additional carbonation on the reduction of the CO_2 diffusion coefficient.

1. Introduction

In current practice, results of normalized carbonation tests at high partial pressures of carbon dioxide (CO_2) (50% P_{atm} in the French [1] standard, 3% P_{atm} in NTBuild-357 [2] or ASTM [3] standards for example) allow the concrete's resistance to carbonation to be characterized but are not fully relevant for predicting the carbonation kinetics under atmospheric carbon dioxide partial pressure (0.03% atmospheric pressure) [18,19]. However, the use of a predictive carbonation model together with these accelerated test results would allow the carbonation kinetics in natural conditions to be assessed from accelerated test results.

At present, the extrapolation from high pressure test results by means of the usual analytical models of the carbonation depth under partial atmospheric pressures is not meaningful. The quantity of carbonated material and the diffusivity of the concrete are expected to be modified with the pressure change [18], and this is generally not accounted for in these models.

Yet researchers, regulation committees and engineers need to have a robust, practical model including the carbon dioxide pressure dependency for their daily practice. The proposed model allows the carbonation depth for different carbon dioxide partial pressures to be estimated from a few data, such as the nature of the cement, the concrete composition and at least one accelerated carbonation test. In this first version, we do not focus on the effect of relative humidity, which is taken as constant and equal to 65%. A following work will address this complex aspect separately.

The laboratory experimental results reported in the first part of this paper demonstrate that the C–S–H carbonation rate and consecutively the CO_2 diffusion coefficient in the carbonated zone depend on the carbon dioxide partial pressure, which leads to a modification of the microstructure (porosity and pore size distribution) and, consequently, of the carbon dioxide diffusion coefficient. In the second part, the previous results are used to build an original but simple model able to predict the carbonation depth at different CO_2 partial pressures.

2. General context

Two types of model for characterizing concrete carbonation that exists at the moment:

- Simple empirical models, which are of the form: $x_c = A\cdot\sqrt{t}$ [4–7], where x_c is the carbonation depth, t is the exposure time and A is a constant depending on the material and the CO_2 partial pressure.
- Enhanced physical models [8–10,20].

The elementary models assume that all the carbonation occurs only on the CO_2 ingress front, which provides the well-known and practical analytical solution proportional to $\sqrt{t}$.

* Corresponding author.
E-mail address: alain.sellier@insa-toulouse.fr (A. Sellier).

0008-8846/$ – see front matter © 2010 Elsevier Ltd. All rights reserved.
doi:10.1016/j.cemconres.2010.06.010

In contrast, the physical models take into consideration the available information about the microstructure and the chemical composition of the concrete. They assume kinetics which can depend on several parameters, such as the carbonatable particle size [9,10] or the progressive chemical evolution of the hydrated cement paste [8]. They are more complex to use in practice (slow numerical procedures) and more difficult to calibrate because of the numerous physical parameters to be fitted by inversed analysis: diffusivity, permeability, isotherms, and pore size distribution [20].

Our goal is therefore to find a compromise between these two types of model. The result has to comply with the physical phenomena in order to properly account for the dependency of C–S–H carbonation rate on the CO_2 pressure, and has to respect two constraints: the model must have an analytical solution and must be easy to fit from an accelerated carbonation test. For this first stage, it is limited to a constant relative humidity condition as noted above.

In the following sections, a description is given of the laboratory tests carried out to reach this goal. The experimental results are then interpreted and lead to a simplified model including the effects of the CO_2 partial pressure.

3. Experimental program

Carbonation tests were performed with three normalized mortars (Table 1), made with the same purely siliceous sand (Leucate), and three types of cement:

- CEM I (52.5 N) — OPC;
- CEM II (A/LL 52.5 N) — clinker and limestone fines;
- CEM III (A 42.5 N) — clinker and slag.

These three cements were chosen because their compositions are significantly different but they have nearly identical specific Blaine surfaces of about 4000 cm^2/g (Tables 2–4). These compositions lead to a total water porosity of the same order for the various mortars as shown in Table 5. Consequently, possible differences between these mortars subjected to carbonation would be attributable only to the nature of their cements (which conditions their initial amount of Portlandite and the refinement of their microstructure).

Mortars were cast in cylinders 11 cm in diameter × 22 cm high. After 90 days of wet curing, core sample cylinders (of diameter 82 mm) were extracted from the original ones in order to avoid wall effects. The core samples were sawed to obtain specimens 8 cm high (Fig. 1).

Then, the lateral faces of the specimens were sealed with self-adhesive aluminum film to ensure unidirectional carbonation.

These specimens were dried in an oven at a temperature of 40 °C to reach a saturation rate in balance with the relative humidity of the carbonation room (65% R.H.). Next, to homogenize the water content in each specimen, they were wrapped in two thicknesses of aluminum film, put in individual plastic bags and kept at a temperature of 40 °C for 28 days.

At the end of this period of homogenization, the saturation profiles were checked by gamma density [10,17] and samples were placed in carbonation chambers with a controlled temperature of 20 °C ± 0.5 °C and relative humidity of 65% ± 5%. Four carbonation chambers were used, each having a different partial pressure of CO_2: atmospheric content (~0.03%), 10%, 25% and 50% maintained by an electronic pressure controller.

Table 1
Composition of mortars.

W/C	C/S
0.5	0.33

Table 2
Composition of CEM I 52.5 N.

Cement clinker		Addition		Specific Blaine surface			
97.5%		2.5%		4180 cm^2/g			
SiO_2	Al_2O_3	Fe_2O_3	CaO	Fire losses	K_2O	Na_2O	SO_3
20.1%	4.9%	3.5%	63.6%	1.1%	1.6%	0.1%	3.5%

Material characterization methods were the following:

- measurement of carbonated thickness by means of phenolphthalein pulverization (colored indicator) at 14 days, 28 days, and 2, 3, 4, 5, 7 and 10 months of exposure;
- X-ray diffraction (XRD) on zones reacting differently to the phenolphthalein;
- thermo gravimetric and thermo differential analyses (TGA/TDA) on healthy and carbonated zones;
- mercury intrusion in healthy and carbonated zones.

4. Limits of elementary models

Fig. 2 gives the carbonation depth versus time for each of the three mortars under study. Each graph includes results at the four CO_2 partial pressures considered.

These results served to fit the classic elementary model based on the assumptions briefly stated below.

The ongoing carbonation is located on the CO_2 ingress front. Taken together with the mass balance of CO_2, and considering CO2 as an ideal gas, this assumption leads to Eq. (1).

$$Q \cdot dx_c = \frac{D_{CO_2}}{R.T} \frac{P_{CO_2}}{x_c} dt \tag{1}$$

With:

–Q: quantity of carbonatable calcium (mol/m^3 of material),
–x_c: carbonated depth (m),
–D_{CO2}: coefficient of CO_2 diffusion in carbonated zones (m^2/s),
–P_{CO2}: pressure of CO_2 at the concrete surface (Pa),
–t: time (s),
–R: constant of perfect gases (J/mol/K),
–T: temperature (K).

In this equation, the amount of CO_2 reaching the carbonation front (x_c) during time dt is completely transformed into calcite by the carbonation reaction in the volume ($1\ m^2 \times dx_c$, see Fig. 3), thus inducing a front advance of dx_c. Note that, at a given time, the gradient of pressure is constant between 0 and x_c and equal to $\frac{P_{CO_2}}{x_c}$. This assumption is a consequence of the CO_2 being consumed only on the front. The integration of the previous equation gives the well-known equation:

$$x_c = \frac{\sqrt{2 \cdot D_{CO_2} \cdot P_{CO_2} \cdot t}}{Q \cdot R \cdot T} \tag{2}$$

Table 3
Composition of CEM II A/LL 52.5 N.

Cement clinker		Addition		Gypsum		Specific Blaine surface	
87.0%		10.0%		3.0%		3922 cm^2/g	
SiO_2	Al_2O_3	Fe_2O_3	CaO	Fire losses	K_2O	Na_2O	SO_3
18.0%	4.6%	2.0%	64.2%	6.2%	0.6%	0.1%	2.7%

Table 4
Composition of CEM III A 42.5 N.

Cement clinker		Addition (slag)		Gypsum	Specific Blaine surface		
56.0%		42.0%		2.0%	3898 cm^2/g		
SiO_2	Al_2O_3	Fe_2O_3	CaO	Fire losses	K_2O	Na_2O	SO_3
20.8%	5.4%	3.1%	65.4%	0.1%	1.0%	0.4%	1.5%

The carbonation depth for a fixed exposure duration t_0 reads:

$$x_c = K \cdot \sqrt{P_{CO_2}} \tag{3}$$

with:

$$K = \sqrt{\frac{2 \cdot D_{CO_2} \cdot t_0}{Q \cdot R \cdot T}} \tag{4}$$

According to this modeling, the constant K is therefore not dependent on the CO_2 partial pressure. If the carbonation depth at a given exposure duration is plotted as a function of the square root of the partial CO_2 pressure, a single straight line should be seen. It is worth noting, though, that the coefficient K estimated from the experimental results obtained under different pressures (for example at $t_0 = 7$ months) is not a constant, but decreases (each straight line in Fig. 4 corresponds to a different value of K). As K depends on the CO_2 pressure (instead of being independent of it as expected in the above theory), we can conclude that the effects of a pressure change are not satisfactorily predicted by the simplified model and Eq. (2) is not suitable for a shift from accelerated tests to natural conditions. A simplified approach to get around this shortcoming could be to use a coefficient K depending on the CO_2 partial pressure in a different way. But, if the underlying physical phenomena are not well understood, the application domain of this new formula could be limited to our own tests. For this reason we chose to perform complementary tests, which are presented and discussed in the following section, and to clarify an enhanced, simplified but physical model considering the effect of the pressure of CO_2 in a more realistic way.

5. Experimental results, interpretations

5.1. Analysis of X-ray diffraction tests (XRD)

Fig. 5 shows the XRD diagrams of the healthy and completely carbonated mortars for two different CO_2 pressures (0.03% P_{atm} and 50% P_{atm}).

For the three types of mortar, it can be seen that the portlandite, the ettringite and the aluminates disappear almost completely from the XRD diagrams for 50% carbon dioxide partial pressure and also for 0.03%. If Q1 denotes the number of moles of calcium initially contained in these three types of hydroxides, then:

$$Q1 = (CH + 4 \cdot AF_m + 6 \cdot AF_t) \cdot \varphi_p \tag{5}$$

Table 5
Porosity for different samples of mortar.

	Mortar type	CEM I	CEM II	CEM III
Water porosity	Healthy mortar	17.2%	17.9%	18.5%
	Healthy mortar	14.4%	13.9%	12.3%
Hg porosity	Carbonated mortar during 296 days under CO_2 atmospheric content	12.9%	12.2%	11.3%
	Mortar carbonated for 157 days under 50% of CO_2	8.8%	10.8%	8.3%

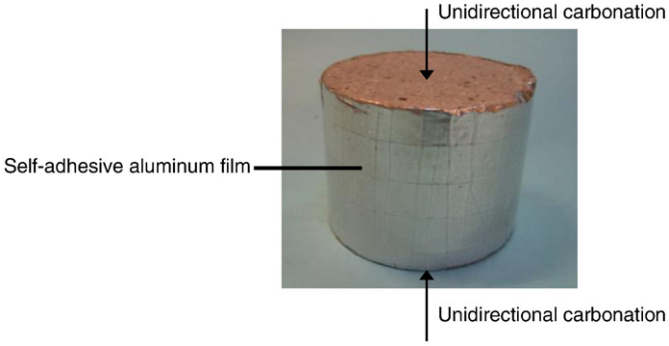

Fig. 1. Unidirectional carbonation principle on sealed specimen.

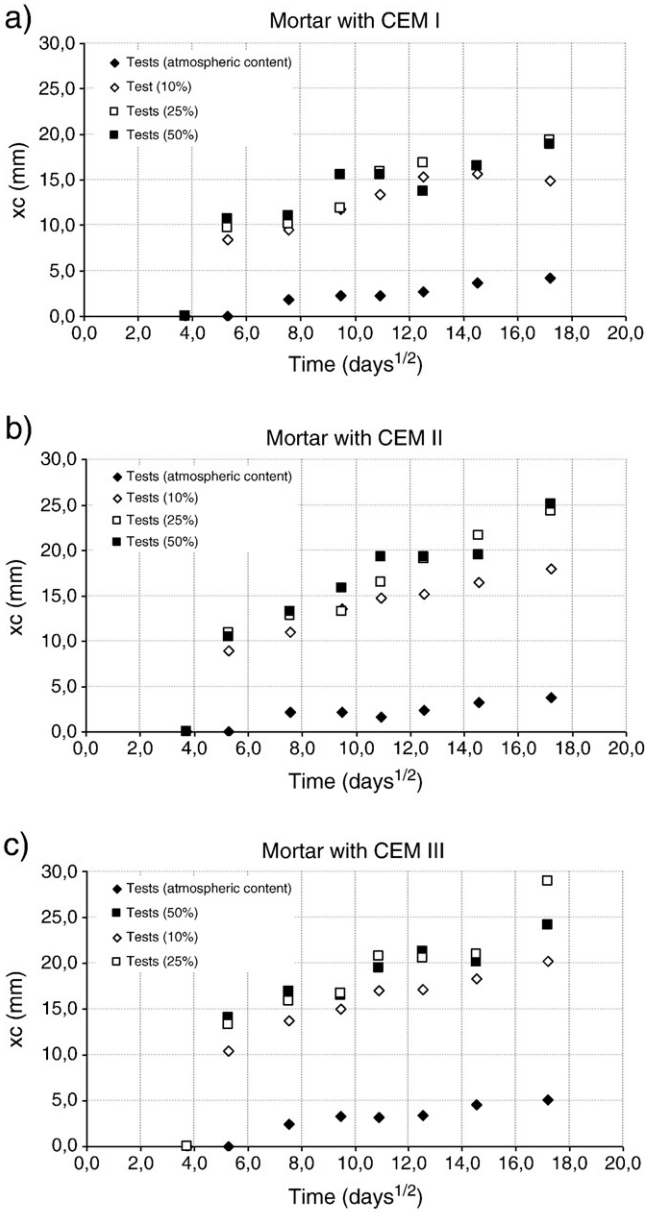

Fig. 2. Evolution of measured carbonated thickness for different mortars and for different CO_2 contents (colored indicator method).

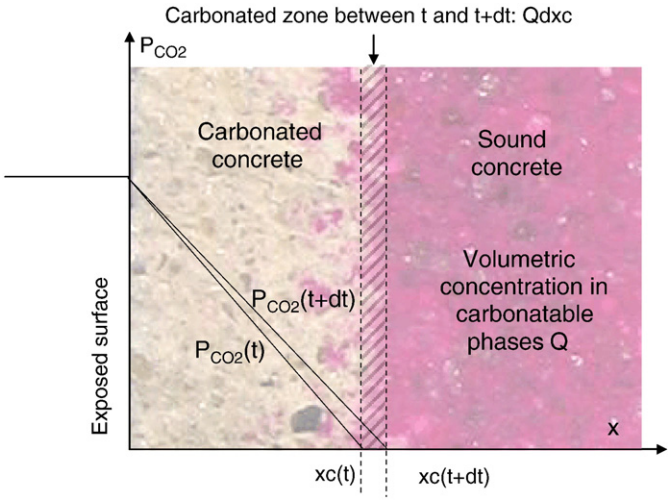

Fig. 3. CO_2 pressure profile and carbonation front ingress in the elementary carbonation theory.

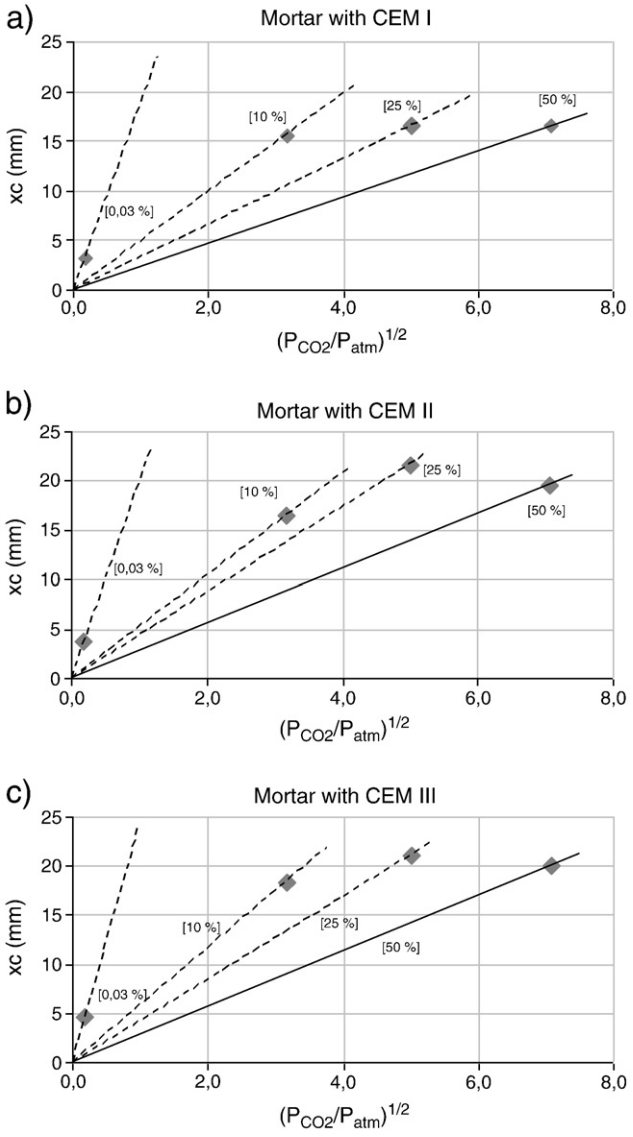

Fig. 4. Carbonation depth at 7 months versus square root of relative CO_2 pressure [X%]. Each straight line corresponds to a different fit for the constant K (cf. Eq. (3)).

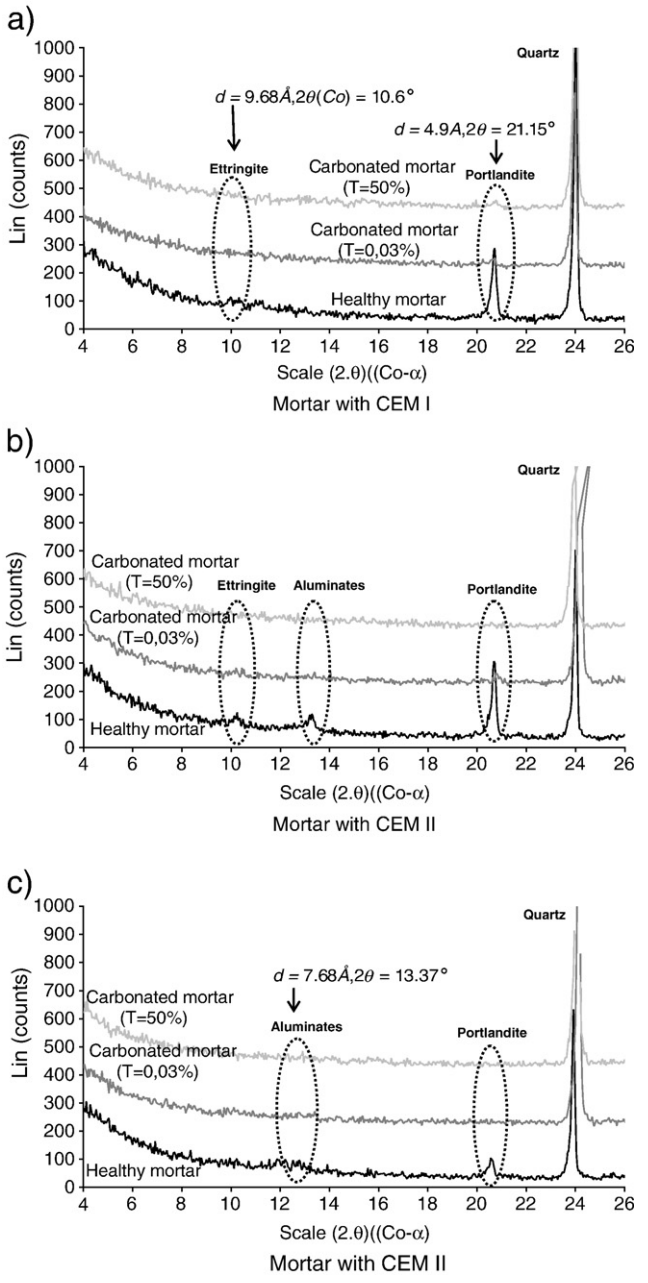

Fig. 5. Analysis of XRD trials for different mortar types (for ease of reading, curves are shifted and normalized with respect to the quartz peak).

with:

- –CH: number of moles of calcium in portlandite (mol/l of cement paste),
- –AFm: number of moles of calcium in monosulfoaluminate (mol/l of cement paste),
- –AFt: number of moles of calcium in ettringite (mol/l of cement paste),
- –φ_p: fraction of paste in the concrete (l of cement paste/l of concrete or mortar).

Hence, Eq. (5) gives the number of moles of calcium that are carbonatable under atmospheric CO_2 content. It will be used in the proposed model.

5.2. Analysis of mercury intrusion tests

Mercury porosities measured on the three mortars are reported in Table 5. Porosities are given either in the healthy zone or in the

completely carbonated zones of the specimens. Tests were carried out according to the GranDuBé method [11]. It can be seen in Table 5 that the porosity of the completely carbonated zone of the mortars decreases when the CO_2 pressure increases. These mercury intrusion tests (given in N. Hyvert's PhD thesis, ref [17]) also showed that the small dimension pores became clogged. Therefore, carbonation reduces the interconnection of the porous network, which should lead to a reduction of the diffusivity coefficient of gaseous CO_2 in the carbonated zone. These porosity changes can be attributed to calcite formation.

Moreover, the previous XRD analyses showed that the portlandite, ettringite and aluminates had been completely carbonated independently of the CO_2 pressure. It is therefore possible to make the following assumption: carbonation of other hydroxides (C–S–H in particular) would be responsible for the volume increase of calcite at high pressure of CO_2, implying a reduction of porosity, as can be seen when comparing the last two lines in Table 5. This assumption agrees with both the XRD analyses and the mercury intrusion tests, and could explain the strong dependency of the diffusion coefficient in the carbonated zone on the partial pressure of CO_2.

5.3. Thermo gravimetric and thermo differential analyses (TGA/TDA)

To confirm the link between the nature of the carbonated hydroxides and the partial pressure of CO_2, TGA/TDA analyses were undertaken on the CEM III mortar (which theoretically initially contained the smallest amount of portlandite). The test was performed according to the GranDuBé method [12].

Although the sample preparation method implied an overevaluation of the carbonation rate (due to crushing in atmospheric conditions), it can be observed in Fig. 6 that less calcite was produced for the mortar initially exposed to the lowest partial pressure of CO_2. When these results were compared with XRD analyses (complete carbonation of portlandite and aluminates under low pressure) and with the reduction of porosity determined in high pressure conditions, it could be deduced that the variation of porosity and of its structure could be explained by a supplementary amount of calcite formed, not resulting from the initial products carbonated at low pressure (portlandite, ettringite and aluminates). This consideration again supports the assumption that the reduction of porosity is due to the carbonation of C–S–H at high pressure of CO_2. This explanation is also in accordance with ref [18].

6. Enhanced elementary model

The quantity Q2 (in mol/l) of carbonated calcium taken from the C–S–H under a given partial pressure of CO_2 is expressed as:

$$Q2 = C2 \cdot f_Q\left(P_{CO_2}\right) \cdot \varphi_p \tag{6}$$

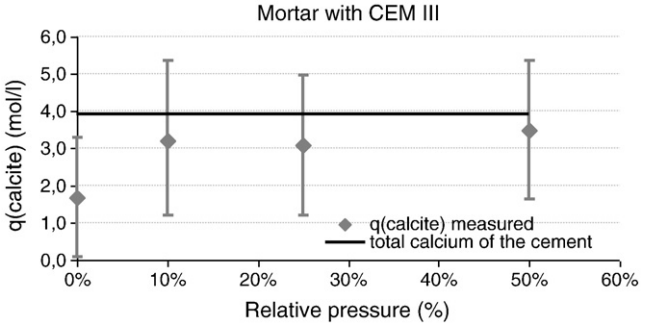

Fig. 6. Analysis of ATD/ATG tests for the mortar with CEM III.

with:

–C2: number of moles of calcium in C–S–H for the material considered (mol/l of cement paste),
–$f_Q(P_{CO_2})$: actual function sought, giving the fraction of carbonated calcium in C–S–H with respect to the exposure pressure (−)
–φp: fraction of paste in the concrete (l of cement paste/l of concrete or mortar).

Moreover, the reduction of porosity attributable to the carbonation of C–S–H could be expressed by a reduction of the diffusivity coefficient, which can be written:

$$D_{CO_2} = \frac{D^0_{CO_2}}{f_D(Q2)} \tag{7}$$

with:

–DCO_2: diffusivity coefficient of CO_2 in carbonated zones for a given CO_2 pressure (m^2/s),
–$D0CO_2$: diffusivity coefficient of CO_2 in carbonated zones for an exposure pressure equal to the natural pressure (0.03% P_{atm}) (m^2/s), ($D^0_{CO_2}$ corresponds to a material where only CH Aft and Afm are carbonated, not the CSH)
–fd(Q2): actual function sought, depending on the quantity of carbonated calcium taken from the C–S–H (−).

When establishing the enhanced elementary model, the quantities of carbonatable calcium Q1 and C2 have to be estimated. Q1 (Eq. (5)) comprises the portlandite, the ettringite and the hydrated ferro-aluminates, and C2 (Eq. (6)) corresponds to calcium included in the C–S–H, in the different mortars studied. To obtain these values as simply as possible, a set of equations based on the mass conservation of oxides during the hydration process was used [13] (Table 6). The hydration degree (α in Eq. (8)) was estimated from the type of cement and the Water/Cement ratio [14,21]. For a CEM I cement, the quantities of each of these solid stages were found by solving the following linear system:

$$\begin{cases} CH + 1.65CSH + 4\,AF_m + 6\,AF_t(ou\,3C3AH6) = \alpha CaO \\ CSH = \alpha SiO_2 \\ 2AF_t(ou\,2C3AH6) + 2\,AF_m = 2\alpha Al_2O_3 \\ 3AF_t(ou\,0C3AH6) + AF_m = \alpha SO_3 \\ \alpha = 1 - \exp(-3.3 \times W/C) \end{cases} \tag{8}$$

With:

–CH: molar quantity of portlandite (mol/l of cement paste),
–CSH: molar quantity of C–S–H (C/S = 1.65) (mol/l of cement paste),
–AFm: molar quantity of monosulfoaluminate (mol/l of cement paste),
–AFt: molar quantity of trisulfoaluminate (mol/l of cement paste),
–C3AH6: molar quantity of hexahydrate (mol/l of cement paste),
–CaO, SiO2, Al2O3, SO3: molar quantities of oxide contents in the anhydrous cement (mol/l cement paste).
– W/C, Water/Cement specific ratio

By default, the system is solved assuming the presence of the ettringite. However, the solving procedure fails if the quantity of sulfates is too weak; in this case, the predominant presence of the

Table 6
Coefficients Q1 and Q2 obtained from oxides of each type of cement.

Mortar with	CEM I	CEM II	CEM III
Q1 (mol/l of concrete)	2.38	2.28	1.19
C2 (mol/l of concrete)	2.26	1.74	2.72

hexahydrate is assumed. In the presence of an anhydrous cement with more iron than aluminum, ferriferous hydroxides are formed, which behave similarly to aluminous hydroxides in the decalcification process and hence may be merged with the latter [16]. For CEM III cements, a chronology in the hydration process is necessary to calculate the ideal composition [13,15]. Firstly, hydration of clinker is considered with a C/S = 1.65 according to Eq. (8) applied to the clinker part of the cement only; next a variant of Eq. (8) is built with C/S = 1 for "secondary CSH" created by "delayed" hydration (of slag in this case), and CaO involved in CH coming from clinker hydration is added to the available CaO able to create "secondary CSH". Note the hydration degree is also modified in this case [21]. The linear system is solved again with these new data and the total amount of hydrate is deduced by combining (according to the global mass balance of oxides) the results coming from these two successive applications of Eq. (8) (Table 6).

The functions f_Q and f_D are proposed as follows (Eqs. (9) and (10)). f_Q is chosen as non-linear but with the restriction of being a power form to allow the integration (Eq. (13)) needed to finally obtain the analytical solution (Eq. (17)). f_D has to be greater than one since it has to reduce the diffusion coefficient if C–S–H are carbonated (see Eq. (7)) and has to increase with the C–S–H carbonation rate, so it is chosen as a simple linear function of the carbonated C–S–H (Q_2).

$$f_Q\left(P_{CO_2}\right) = \left(\frac{P_{CO_2}}{P_{atm}}\right)^n \tag{9}$$

$$f_D(Q2) = 1 + \frac{\beta.}{\varphi_p} Q2 \tag{10}$$

where n and β are two parameters to be fitted. As the cement nature and its dosage in the concrete mix have already been taken into account through the quantities Q1 and C2, n and β are expected to be independent of the concrete composition and of the cement nature. "n" reflects only the "chemical affinity" of C–S–H towards the CO_2 pressure condition, while β reflects the supplementary sealing of porosity due the C–S–H carbonation.

The introduction of these functions in the one-dimensional mass balance equation of gaseous carbon dioxide gives the following partial differential equation:

$$\underbrace{\frac{\varphi_g}{R.T}\frac{\partial P_{CO_2}}{\partial t}}_{A} = \underbrace{\frac{\partial}{\partial x}\left(\frac{D^0_{CO_2}}{R.T\cdot\left(1+\beta\cdot C_2\cdot\left(\frac{P_{CO_2}}{P_{atm}}\right)^n\right)}\cdot\frac{\partial P_{CO_2}}{\partial x}\right)}_{B} + \underbrace{\left(\varphi_p\frac{C_2}{P_{atm}}\cdot\left(\frac{P_{CO_2}}{P_{atm}}\right)^{n-1}\right)\cdot\frac{1}{R.T}\frac{\partial P_{CO_2}}{\partial t}}_{C} \tag{11}$$

With:

A: term representing the CO_2 concentration variation in the porosity
B: diffusion term
C: CO_2 consumed by the CSH

In Eq. (11), as β and n are assumed independent of the cement type, only D_0 (diffusivity coefficient in carbonated zones for atmospheric pressure) is influenced by the porosity of the cement paste. Eq. (11) must be solved with the following boundary conditions:

$$\begin{cases} P_{CO_2}(0,t) = P_0 \\ -\dfrac{D_{CO_2}}{R.T}\cdot\left(\dfrac{\partial P_{CO_2}}{\partial x}\right)_{x=x_c} = Q1\cdot\dfrac{dx_c}{dt} \end{cases} \tag{12}$$

where x_c is the depth of the carbonated zone. The last of the boundary conditions takes into account the fact that the quantity Q1 is not modified by the pressure of CO_2. Under low pressure conditions, the solution of Eq. (11) merges with the classic solution, proportional to the square root of time. If the boundary pressure, P_{CO_2}, is increased, the solution moves away from this reference solution. However, an approximate solution can be proposed if the amount of CO_2 consumed between x = 0 and $x = x_c$ is expressed as:

$$I2 = \varphi_p \int_0^{xc} C2\cdot\left(\frac{P_{CO_2}}{P_{atm}}\right)^n dx \tag{13}$$

In addition, if the profile of the carbonation front is approximated linearly, which is very realistic under low pressure as explained above, and expressed as:

$$P_{CO_2} = P_0\cdot\left(\frac{x_c - x}{x_c}\right) \tag{14}$$

then we have:

$$I2 = \varphi_p\frac{C2}{n+1}\cdot\left(\frac{P_0}{P_{atm}}\right)^n\cdot x_c \tag{15}$$

A global mass balance is now made on the whole carbonated zone. It consists in stating that the CO_2 flux entering the concrete at x = 0 serves (i) to increase I2 and (ii) to act on the carbonation front, making it slip forward, which is written as:

$$\frac{D^0_{CO_2}}{R.T\cdot\left(1+\beta\cdot C2\cdot\left(\frac{P_0}{P_{atm}}\right)^n\right)}\frac{P_0}{x_c}\cdot dt = \left(\frac{\varphi_p.C2}{n+1}\cdot\left(\frac{P_0}{P_{atm}}\right)^n + Q1\right)dx_c \tag{16}$$

The main advantage of the aforementioned approximations is that they lead to the analytical Eq. (16) being explicitly integrable, and thence to the expression for the carbonation depth (Eq. (17)):

$$x_c(t) = \sqrt{\frac{2\cdot D^0_{CO_2}\cdot P_0\cdot t}{R.T\cdot\left(1+\beta\cdot C2\cdot\left(\frac{P_0}{P_{atm}}\right)^n\right)\cdot\left(\frac{\varphi_p.C2}{n+1}\cdot\left(\frac{P_0}{P_{atm}}\right)^n + Q1\right)}} \tag{17}$$

This equation still gives a carbonation depth as a function of the square root of the time but this function is no longer a square root of the CO_2 pressure. This is the main consequence and enhancement of the model; the pressure acts differently on the kinetics than in Eq. (2).

7. Fitting model parameters

The following three model parameters have to be fitted:

–$D0CO_2$: diffusion coefficient of CO_2 under atmospheric partial pressure of CO_2. It is the only parameter depending on the material considered (m^2/s), and has to be fitted for each new material, from an accelerated carbonation test for instance.
–β: independent of the material,
–n: also independent of the material.

Table 7
Model parameters.

Mortar with	CEM I	CEM II	CEM III
$D^0_{CO_2}$ (10^{-8} m^2/s)	5.7	6.0	7.2
β (l/mol)	7.76		
n	0.67		

After a fitting procedure based on the least squares method including all the experimental results (the three cements, the four CO_2 pressures and all the times of observation of the depth in the tests), the following parameter values were obtained (Table 7).

As expected, a single set of parameters n and α allowed acceptable adjustment of all the experimental results. Fig. 7 illustrates the adjustment quality. As a consequence of approximation (14) needed to obtain analytical solution (17), the model is particularly efficient at low pressure and the adjustment quality decreases with higher pressure. A better fitting can be obtained without approximation (14) but requires numerical integration of Eq. (11) with Eq. (12) as boundary conditions. The analytical result (Eq. (17)) then appears as a good compromise between accuracy and ease of use for practitioners. Fig. 8 shows the benefit of the approach in terms of the dependency on CO_2 partial pressure. The relationship, at a given exposure time, is no longer linear as in Fig. 2, but non-linear, in acceptable accordance with the experimental results. This non-linearity is also in accordance with previous "empirical models" [7].

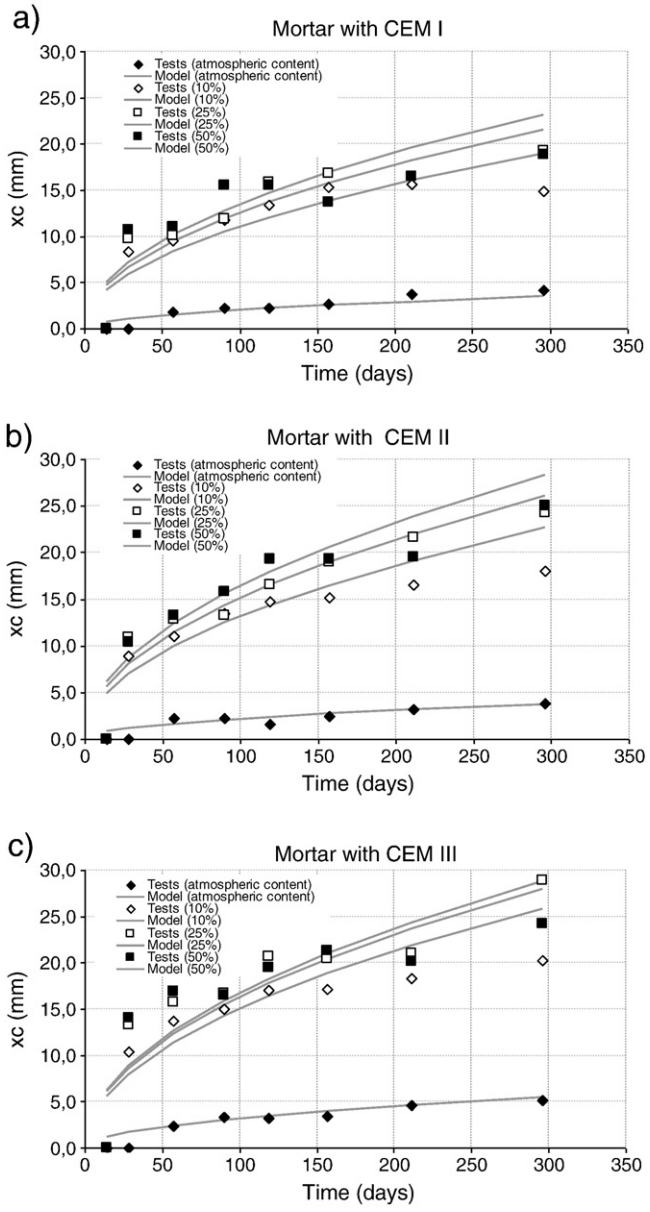

Fig. 7. Confrontation of the model with the experimental points for different CO_2 rates (0.03%, 10%, 25% and 50%).

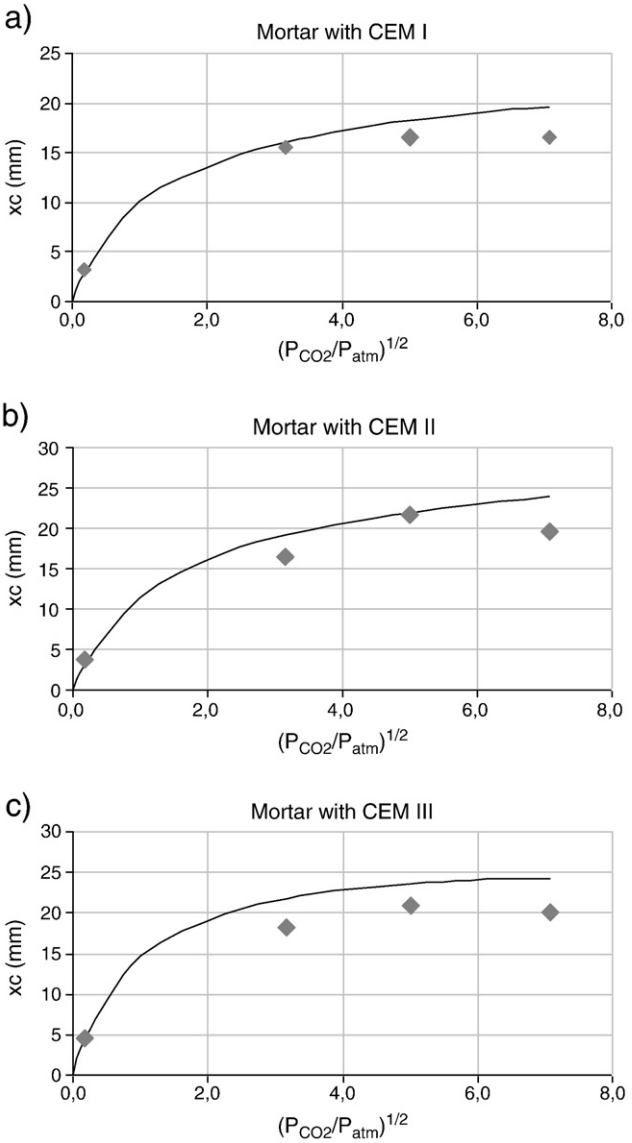

Fig. 8. Comparison of experiments with different CO_2 contents [X] in 211 days with the model worked out for different types of mortar.

8. Conclusions and perspectives

The objective of this paper was to propose an elementary model to predict carbonation under various CO_2 partial pressures from results obtained with an accelerated test. A comprehensive experimental program was carried out, including four rates of CO_2 partial pressure (0.03%, 10%, 25% and 50% of P_{atm}), three types of mortar and cement, seven exposure times (up to 300 days) at which the carbonated depth and mercury porosity were measured, together with XRD and DTA/TGA analyses.

The comparison between the experimental carbonation depth and its theoretical value given by a simple model based on the assumption of a steep slope carbonation front revealed that the shift from high pressure tests to natural conditions was not satisfactorily addressed by this kind of model.

The XRD analyses showed that the portlandite, ettringite and aluminates were effectively widely carbonated at low pressure. But the mercury intrusion analyses showed that the porosity decreased in the carbonated zone when the CO_2 pressure increased. From the DTA/TGA analyses, it was noted that the decrease of porosity was linked to the higher carbonation under the high pressures than at the low

pressures. Finally, from a cross-analysis of XRD and DTA/TGA outputs, it was found that the C–S–H carbonation rate depended on the CO_2 partial pressure.

Consequently, an elementary model was proposed, rationally bringing together all these observations, in which the quantity of carbonated calcium had two sources:

–The calcium of the portlandite, the ettringite and the aluminates. This calcium is completely carbonatable whatever the CO_2 partial pressure;
–The calcium of CSH. The carbonation rate is given by a function $(P_{CO_2}/P_{atm})^n$ coming from fitting on three types of cement and four levels of pressure.

Moreover, the change in the diffusion coefficient related to calcite formation under high pressures was also taken into account by a simple relationship.

An approximate solution of the carbonation front ingress kinetics was then proposed. Only three parameters (n, α and $D^0_{CO_2}$) were involved in the solution and enabled it to comply with all the experimental results.

An immediate follow-on from this work would consist in testing the reliability of this approach for other mortar or concrete varieties. Beyond that, a second experimental plan is currently being finalized to take account of the effects of humidity and temperature conditions different from those of the tests performed here (20 °C and 65% of relative humidity). The results and the model adaptations induced will be proposed in a following publication. This will allow the model to be applied to natural conditions, which is the final aim.

References

[1] XP P 18-458 standard, Essai pour béton durci – Essai de carbonatation accélérée – Mesure de l'épaisseur de béton, 2008.
[2] NT Build 357, "Concrete, repairing materials and protective coating UDC: carbonation resistance" 691.32:658.588, Published by NORDTEST Tekniikantie 12, FIN-20150 Espoo, FINLAND, ISSN 0283-7153, approved 11-1989. http://www.nordicinnovation.net/nordtestfiler/build357.pdf.
[3] ASTM C876-91, 1999, Standard test method for half-cell potential of uncoated reinforcing steel in concrete, annual book of ASTM standard, vol. 03 02, pp 462–467.
[4] Duracrete, Probabilistic Performance Based Durability Design of Concrete Structures, Brite Euram Project, 1999 n°1347.
[5] V.G. Papadakis, C.G. Vayenas, M.N. Fardis, Fundamental modelling and experimental investigation of concrete carbonation, ACI Materials Journal 88 (n° 4) (1991) 363–373.
[6] V.G. Papadakis, C.G. Vayenas, M.N. Fardis, Experimental investigation and mathematical modelling of the concrete carbonation problem, Chemical Engineering Science 46 (1991) 1333–1338.
[7] K. Sisomphon, L. Franke, Carbonation rates of concretes containing high volume of pozzolanic materials, Cement and Concrete Research 37 (2007) 1647–1653.
[8] B. Bary, A. Sellier, Coupled moisture-carbon dioxide-calcium transfer model for carbonation of concrete, Cement and Concrete Research 34 (2004) 1859–1872.
[9] M. Thiery, 2005, "Modélisation de la carbonatation atmosphérique des bétons – Prise en compte des effets cinétiques et de l'état hydrique", PhD thesis, Ecole Nationale des Ponts et Chaussées.
[10] M. Thiery, G. Villain, P. Dangla, G. Platret, Investigation of the carbonation front shape on cementitious materials: effects of the chemical kinetics, Cement and Concrete Research 37 (2007) 1047–1058.
[11] GranDuBé, Mesures par intrusion de mercure, Association Française de Génie Civil, 2007, pp. 335–344, Chap II.1.
[12] GranDuBé, Détermination de la perte au feu, Association Française de Génie Civil, 2007, pp. 309–310, Chap II.1.
[13] A. Sellier, Modélisations numériques pour la durabilité des ouvrages de génie civil, Habilitation à Diriger des Recherches, Université Paul Sabatier, Dec. 12 2006.
[14] L. Buffo-Lacarrière, A. Sellier, G. Escadeillas, A. Turatsinze, Multiphasic finite element modeling of concrete hydration, Cement and Concrete Research 37 (2007) 131–138.
[15] F. Adenot, Durabilité des bétons : caractérisation et modélisation des processus physiques et chimiques de dégradation du ciment. PHD thesis of the University of Orléans 1992 (in French).
[16] M. Collepardi, M. Corradi, Tetracalcium aluminoferrite hydration in the presence of lime and gypsum, Cement and Concrete Research 9 (1979) 431–437.
[17] N. Hyvert, 2009, "Application de l'approche probabiliste à la surabilité des produits préfabriqués en béton", PhD thesis, Université de Toulouse, April 2009 (in French).
[18] CastelloteM. , FernandezL. , AndradeC. , AlonsoC. , Chemical changes and phase analysis of OPC pastes carbonated at different CO_2 concentrations, Materials and Structures (2008), doi:10.1617/s11527-008-9399-1 RILEM.
[19] M.A. Sanjuán, C. Andrade, M. Cheyrezy, Concrete carbonation tests in natural and accelerated conditions, Advances in Cement Research 15 (4) (October 2003) 171–180 Print ISSN: 0951-7197.
[20] T. Ishida, K. Maekawa, M. Soltani, Theoretical identified strong coupling of carbonation rate and thermodynamic moisture state in micropores of concrete, Journal of Advanced Concrete Technology 2 (n°2) (2004) 213–222.
[21] V. Waller (1999), "Relation entre composition des bétons, exothermie en cours de prise et résistance en compression", PHD Thesis, ENPC, Paris, 297p. (in French).